Electrochemical Performance and Electrocatalytic Behavior of Myoglobin Modified TiO₂@3D Graphene Composite Electrode

Yunxiu Sun[1], Wei Chen[1], Xiaoqing Li[2], Qinyang Yu[2], Yuxin Zhu[2], Yitong Wang[2],
Lin Chen[2], Wei Sun[2], Guangjiu Li[1,*], Yanyan Niu[2,*]

[1] Key Laboratory of Optic-electric Sensing and Analytical Chemistry for Life Science of Ministry of Education, College of Chemistry and Molecular Engineering, Qingdao University of Science and Technology, Qingdao 266042, P. R. China
[2] Key Laboratory of Laser Technology and Optoelectronic Functional Materials of Hainan Province, Key Laboratory of Functional Materials and Photoelectrochemistry of Haikou, College of Chemistry and Chemical Engineering, Hainan Normal University, Haikou 571158, China
[*]E-mail: lgjqust@126.com; 792366546@qq.com

In the study titanium dioxide (TiO_2) doped three-dimensional graphene (3DGR) nanocomposite $(TiO_2@3D\ GR)$ was prepared via a one-step hydrothermal synthesis method. SEM results showed a three-dimensional network structure with TiO_2 particles uniformly loaded in the graphene pores. Using PBS with different pH values as supporting electrolyte, the influence of acid-base property on the electrochemical experiments based on the proposed biosensor (Nafion/Mb/TiO₂@3DGR/CILE) was investigated. The effect of sweep speed on electrochemical behavior was further explored. Nafion/Mb/TiO₂@3DGR/CILE showed good electrocatalytic activity for trichloroacetic acid, $NaNO_2$ and H_2O_2 with K_M^{app} as 107.12 mM, 31.53 mM and 34.23 mM, obtaining wider range of linearity and lower limit of detection. The biosensor is of important significance for future research and development of electrochemical biosensor.

1. INTRODUCTION

As one of the myocardial markers of acute myocardial infarction, the increase of Mb content in plasma reflects the severity of myocardial injury to a certain extent [1-3]. Therefore, it is important to monitor the Mb content, which is released by cardiomyocytes accurately and effectively in advance [4]. Due to its known structure, commercial availability, and relatively low molecular weight, Mb is an ideal heme-protein that plays an important role in biological processes. However, the redox active site

[Fe(III)/Fe(II)] of Mb is deeply embedded in the molecular structure, making direct electron transfer of Mb difficult at conventional electrodes [5]. Therefore, nanomaterials are generally used to modify electrodes, providing an appropriate load substrate for Mb electron transfer. Traditional electrochemical enzyme biosensors have played an indelible role in monitoring a variety of biomarkers owing to their low production cost and high sensitivity. Due to many problems existing in the traditional enzyme immobilization methods, various procedures are often taken, such as finding suitable materials and effective loading of enzymes. [6-8].

Recently, graphene has been widely used in environmental pollutant degradation [9, 10], brine recovery [11, 12], lithium-ion battery design [13-15], impurity absorption in water [16, 17], and other fields. Graphene has large theoretical specific surface area and excellent electrical conductivity, which is often used as electrode modification material for electrochemical biosensors [18-20]. However, the stacking of graphene sheets not only inhibit its high electrical conductivity, but also affect electron transfer [21]. To remedy these shortcomings, researchers focus on synthesizing graphene with three-dimensional (3D) networked structures [22, 23]. The 3D mesh graphene has lower density, higher specific surface area and porosity as compared with two-dimensional (2D) graphene, which makes it an ideal carrier for electrochemical enzyme sensors. In addition, 3DGR shows a continuous multi-space structure in terms of rapid mass transfer and electron dynamics, so it can be used as materials for improving the electrochemical performance of biosensors [24]. Shen et al. prepared 3D GR-based nanomaterials with large mesoporous structures as carrier for novel enzyme electrodes [25]. Fu et al. developed a multistage multi-void partial graphite-carbon film with 3D network nanoscale channels and used it as a monolithic substrate for electrochemical biosensors [26].

Titanium dioxide (TiO$_2$) is an N-type wide band gap semiconductor [27, 28] with advantages of chemical stability, low price, large specific surface area, good biocompatibility [29, 30] and so on, which has become a research hotspot in the field of sensors [31-33]. In this work, TiO$_2$@3DGR nanocomposite was synthesized in situ by hydrothermal method. By using carbon ionic liquid electrode (CILE) as the substrate electrode, Nafion/Mb/TiO$_2$@3DGR/CILE was prepared and followed by the investigations on its electrochemical behaviors. The nanosized TiO$_2$ particles were uniformly loaded on the 3D porous network graphene, which combined the advantages of TiO$_2$ and 3DGR to form a sensing interface with large specific surface area and good electrical conductivity. It is also in favor of Mb immobilization on the interface with its original secondary structure and biological activity remained, which has some inspiration for the exploitation of enzyme biosensors. The structure diagram of Mb and the manufacturing flow chart of this biosensor are shown in Figure 1.
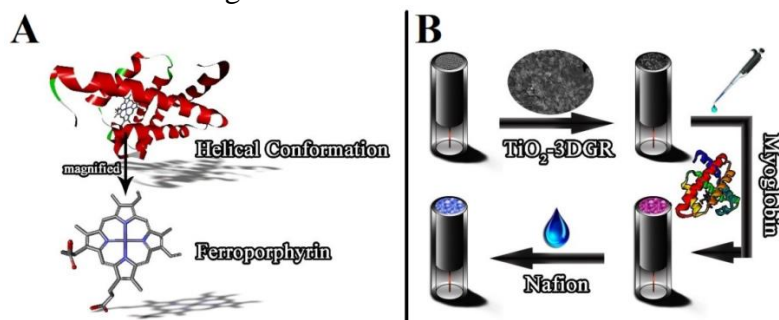

Figure 1. **(A)** Helical conformation of Mb and magnified ferroporphyrin; **(B)** Flowchart of fabrication process of this Nafion/Mb/TiO$_2$@3DGR/CILE.

2. EXPERIMENTAL SECTION

2.1 Apparatus and equipment

Electrochemical experiments were completed on CHI 604E electrochemical workstation (Shanghai Chenhua Instrument, China). By using standard three-electrode system, working electrode (Nafion/Mb/TiO$_2$@3DGR/CILE) was prepared in the laboratory with saturated calomel electrode (SCE) as reference electrode and platinum electrode as auxiliary electrode. Scanning electron microscopy (SEM) images were executed by a JSM-7100F (JEOL, Japan) microscope.

2.2 Reagents

1-Hexylpyridine hexafluorophosphate (HPPF$_6$, Lanzhou Yulu Fine Chemical Co., Ltd., China), GO aqueous solution (8.0 mg/mL, Institute of Coal, Chemistry Chinese Academy of Sciences), TiO$_2$ (Aladdin Reagents Co., Ltd., China), graphite powder (average particle size≤30 μm, Shanghai Colloidal Chemical Factory, China), Mb (MW:17800, Sinopharm Chemical Reagent Co., Ltd., China), Nafion (5.0% ethanol solution, Sigma-Aldrich, USA), TCA (Tianjin Kemiou Chem. Co., Ltd., China), NaNO$_2$ (Shanghai Chemical Reagent Factory, China), 30% H$_2$O$_2$ (Xilong Scientific Co., Ltd., China). The reagents used in this experiment are analytical purity and the experimental water is ultrapure water. The electrolyte solution was deoxygenated with N$_2$ for 45 min before each experiment.

2.3 Synthesis of TiO$_2$@3DGR

40.0 mg TiO$_2$ and 2.0 mg/mL GO solution (20 mL) were mixed by ultrasonic treatment for 1 h, and then transferred into 50 mL Teflon lined reactor. By keeping at 180°C for 2 h, black cylinder was obtained after natural cooling, then freeze-dried at -88°C for 12 h to obtain TiO$_2$@3DGR.

2.4 Preparation of Nafion/Mb/TiO$_2$@3DGR/CILE

Based on the literature [34], CILE was easy to prepare with the details as follows. Graphite powder (1.6 g) and HPPF$_6$ (0.8 g) were grinded with appropriate amount of liquid paraffin for 1h, then loaded into the glass tube (Φ=4 mm) and compacted. Then a copper wire was inserted and the electrode surface was polished on the grinding paper until smooth.

The working electrode was modified by direct drop coating method with the detailed described below. 8.0 μL 2.0 mg/mL TiO$_2$@3DGR suspension was dropped on the surface of the newly prepared CILE, and then 8.0 μL 15.0 mg/mL Mb was coated with 0.5 % Nafion ethanol dilution to successfully prepare Nafion/Mb/TiO$_2$@3DGR/CILE. Other similar modified electrodes such as Nafion/CILE, Nafion/Mb/CILE and Nafion/TiO$_2$@3DGR/CILE were also fabricated by similar methods.

3. RESULTS AND DISCUSSION

3.1 Morphology characterization of TiO₂@3DGR

SEM of TiO$_2$@3DGR nanocomposite at different magnifications was shown in Figure 2. The graphene with network structure was clearly visible and the three-dimensional holes of graphene proved the formation of 3DGR (Figure 2A), which is consistent with the literature [35]. Also TiO$_2$ was loaded on it with uniform size and wrapped by 3DGR network structure, which proved the interconnected of TiO$_2$ nanoparticles with GR nanosheets (Figure 2B-D). TiO$_2$@3DGR nanocomposite combined the advantages of good biocompatibility of TiO$_2$ and huge pore surface area of 3DGR, which provided the possibility for adsorbing more Mb molecules.
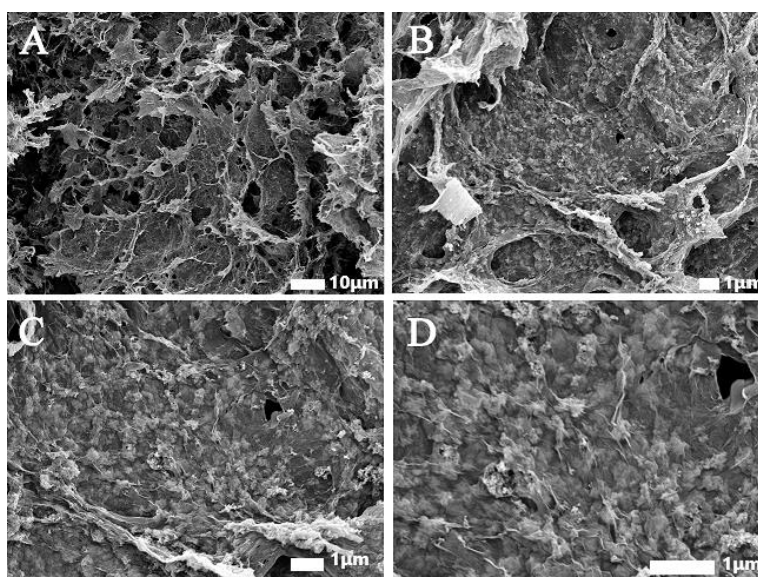

Figure 2. SEM images of (A) 3DGR and (B-D) TiO$_2$@3DGR with different magnifications.

3.2 Direct electrochemistry of Mb

Figure 3A represented CV curves of different modified electrodes in pH 4.0 buffer at scan rate of 0.1 V·s^{-1}. There are no peak appeared on Nafion/CILE (curve d) and Nafion/TiO$_2$@3DGR/CILE (curve b), indicating that no electrochemical active material was present on the modified electrode. Compared with Nafion/CILE, Nafion/TiO$_2$@3DGR/CILE showed higher background current. A pair of asymmetric peaks on Nafion/Mb/CILE (curve c) indicated the direct electron transfer between Mb and CILE. On Nafion/Mb/TiO$_2$@3DGR/CILE (curve a), a pair of symmetrical peaks appeared with the peak current increased. The results show that the modification of TiO$_2$@3DGR accelerated the electron transfer rate between Mb and electrode interface, which may be attributed to the porous and high conductive TiO$_2$@3DGR enhancing the loading capacity of Mb. It can be observed that Epa and Epc were -0.199V and -0.315V (vs. SCE, curve a) with $\triangle$Ep as 116 mV and E$^{0'}$ as -0.257 V (*vs.* SCE),

which were close to the reported values [36, 37]. And the redox peak current ratio was close to 1, showing the characteristic electrochemical behavior of Fe(III)/Fe(II) in Mb.

Electrochemical impedance spectroscopic (EIS) results are shown in Figure 3B and the diameter of high frequency semicircle can reflect the influence on electron transfer rate after modification of electrodes. The larger diameter indicates the larger impedance value (Ret) with the slower electron transfer speed. On the contrary, smaller Ret value leads to faster electron transfer. EIS of Nafion/TiO$_2$@3DGR/CILE (curve a), Nafion/Mb/TiO$_2$@3DGR/CILE (curve b), CILE (curve c), Nafion/CILE (curve d) and Nafion/Mb/CILE (curve e) were recorded with the results shown in Figure 3B. Ret of Nafion/TiO$_2$@3DGR/CILE (curve a) was the smallest of all modified electrodes, which was due to high conductivity of TiO$_2$@3DGR. Ret value of CILE (curve c) was 78.36 Ω and increased to 105.86 Ω after modified by Nafion (Nafion/CILE, curve d), which was due to the non-conductivity of Nafion. The Ret of Nafion/Mb/CILE (curve e) increased to the maximum of 174.45 Ω, which was ascribed to polypeptide chain of Mb hindering communication between Fe electroactive center and electrode. The Ret of Nafion/Mb/TiO$_2$@3DGR/CILE (curve b) was 60.55 Ω, which was reduced significantly compared with Nafion/Mb/CILE (curve e), Nafion/CILE (curve d) as well as CILE (curve c). The above results indicated that the porous TiO$_2$@3DGR with high conductivity played a promoting role in the electron transfer. Meanwhile, the interaction between TiO$_2$@3DGR and Mb may enhance the electronic communication.
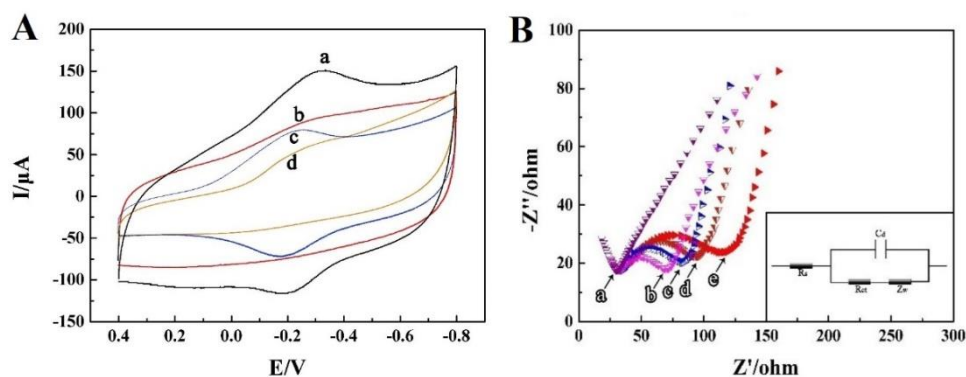

Figure 3. (A) CVs of (a) Nafion/Mb/TiO$_2$@3DGR/CILE, (b) Nafion/TiO$_2$@3DGR/CILE, (c) Nafion/Mb/CILE, (d) Nafion/CILE in pH 4.0 buffer at a scan rate of 0.1 V·s^{-1}; (B) EIS pattern: (a) Nafion/TiO$_2$@3DGR/CILE, (b) Nafion/Mb/TiO$_2$@3DGR/CILE, (c) CILE, (d) Nafion/CILE, and (e) Nafion/Mb/CILE in a 10.0 mM [Fe(CN)$_6$]$^{3-/4-}$ and 0.1 M KCl mixed solution with frequency from 10^4 to 0.1 Hz (inset is the Randles circuit model in the cell).

3.3 Electrochemical behaviors

As shown in Figure 4A, the effect of electrochemical kinetics of Nafion/Mb/TiO$_2$@3DGR/CILE was further explored. A pair of redox peaks appeared with different sweep speeds (0.1~0.6 V·s^{-1}), along with positive and negative shifts of E$_{pc}$ and E$_{pa}$ respectively as the sweep speed increased. The anodic potential tended to shift towards positive direction because of the polarization phenomenon in the CV experiment, while the cathode potential tended to the negative direction, which proved a quasi-reversible reaction process. I$_{pa}$ and I$_{pc}$ also increased with sweep speed

increased, which indicated a typical thin-layer controlled electrochemistry process. Figure 4B displayed the linear regression equations between I_p and υ as I_{pa} (μA) = -159.27 υ (V·s^{-1}) - 2.085 (n=11, R^2=0.996) and I_{pc} (μA) = 230.63 υ (V·s^{-1}) - 1.360 (n=11, R^2=0.998), respectively. The linear regression equations of E_p and lnυ were shown in Figure 4C as E_{pc} (V) = -0.0529 ln υ (V·s^{-1}) - 0.379 (n=11, R^2=0.994) and E_{pa} (V) = 0.0432 ln υ (V·s^{-1}) - 0.0150 (n=11, R^2=0.999). According to the formula and the slope ratio of linear regression equation of E_p and ln υ, the electron transfer number (n), the electron transfer coefficient (α) and reaction rate constant (k_s) were calculated as 1.08, 0.45 and 0.68 s^{-1} respectively. Compared with the reference [38] (k_s = 0.234 s^{-1}), the larger k_s value indicated that the modification of TiO$_2$@3DGR made the electronic exchange between Mb and the electrode surface faster, which provided a favorable conductive electronic sensing platform.

On the basis of the formula $Q=nAF\Gamma^*$ (where Q represented the charge quantity, A was electrode geometry area, F was Faraday constant, n was electrode transfer number of the reaction and Γ^* stood for the absorption of Mb on the surface of the electrode), Γ^* was calculated 1.43×10^{-8} mol·cm^{-2}, that was, the Mb molecules actually involved in chemical reaction accounted as 26.72% of the total of Mb molecules on the electrode surface. Therefore, TiO$_2$@3DGR offers more opportunities for the loading of Mb molecules for the electron transfer.

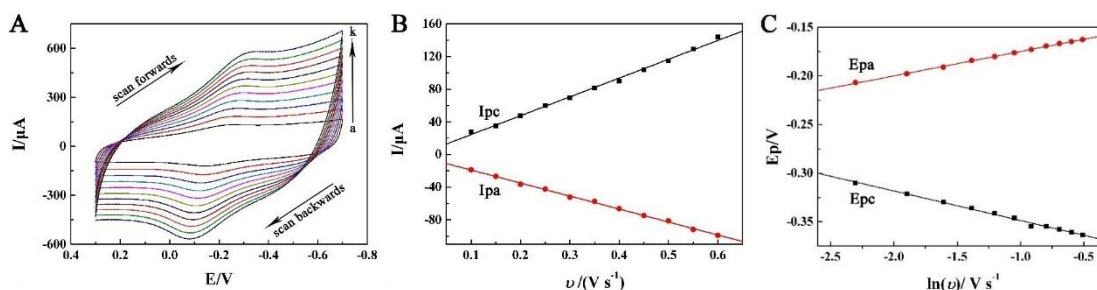**Figure 4.** (A) CVs of Nafion/Mb/TiO$_2$@3DGR/CILE with different scan rates (a → k: 100, 150, 200, 250, 300, 350, 400, 450, 500, 550, 600 mV·s^{-1}) in pH 4.0 buffer; (B) Linear relationship between redox currents and scan rate (υ); (C) Linear relationship between redox peak potentials and ln υ.

3.4 Electrocatalytic behavior of Nafion/Mb/TiO$_2$@3DGR/CILE

The detection of TCA has become a research focus in recent years since TCA is difficult to be decomposed naturally, thus it is significance to design a sensitive, rapid and efficient biosensor to detect TCA. Figure 5A showed the electrocatalytic experiments of TCA by Nafion/Mb/TiO$_2$@3DGR/CILE. The reduction peak at -0.309 V was observed and increased as TCA was gradually added to the buffer. On the contrary, the oxidation peak current decreased with the increase of C$_{TCA}$ and finally disappeared. Also a new peak appeared at -0.579 V, which could be explained by the electrocatalytic mechanism [39]. With the increase of C$_{TCA}$, I$_{pc}$ also increased in proportion and the good linear regression equation with C$_{TCA}$ in the range of 10.0 to 150.0 mM was I (μA) = 4.869 C$_{TCA}$ (mM) + 19.75 (n=15, γ=0.998) with the detection limit as 0.33 mM (3σ), which was

smaller than the reported value of 1.33 mM [40] and 0.615 mM [41]. I_{pc} reached a platform while C_{TCA} was higher than 150.0 mM, showing the Michaelis-Menten dynamic mechanism. K_M^{app} is a vital criterion to investigate the kinetics of the reaction between enzyme and substrate in enzymatic reaction, which can be measured by using the Lineweaver-Burk equation as follows:

$$\frac{1}{I_{SS}} = \frac{1}{I_{max}} + \frac{K_M^{app}}{I_{max}C}$$

I_{ss} represents the transient steady-state current of different C_{TCA} in the linear interval, C is C_{TCA} and I_{max} is the maximum saturation current value when C_{TCA} was greater than 150.0 mM. The K_M^{app} of Nafion/Mb/TiO$_2$@3DGR/CILE for TCA was calculated as 107.12 mM.
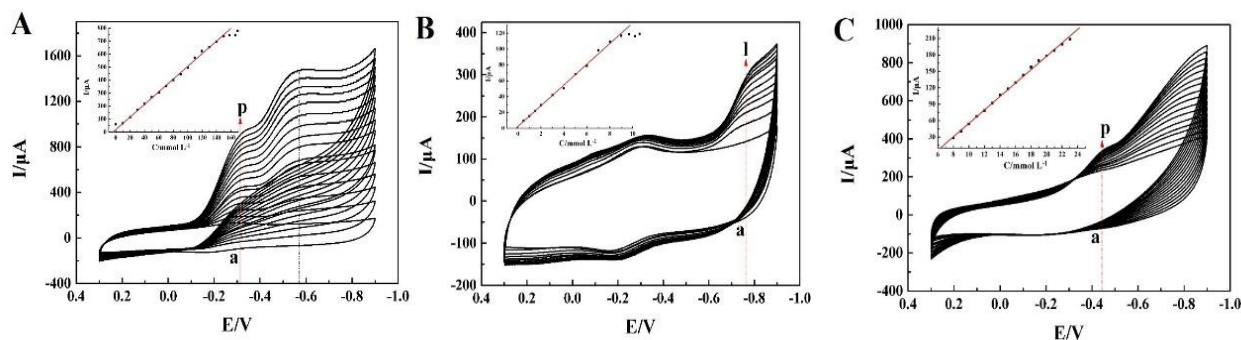

Figure 5. CVs of Nafion/Mb/TiO$_2$@3DGR/CILE with different concentrations of (A) TCA (a → p : 0.0, 10.0, 20.0, 30.0, 40.0, 50.0, 60.0, 70.0, 80.0, 90.0, 100.0, 110.0, 120.0, 130.0, 140.0, 150.0 mM; inset is the linear relationship of Ipc and TCA concentration); (B) NaNO$_2$ (a → k : 0.5, 1.0, 1.5, 2.0, 3.0, 4.0, 5.0, 6.0, 7.0, 8.0, 9.0 mM; inset is the linear relationship of I$_{pc}$ versus NaNO$_2$ concentration); (C) H$_2$O$_2$ (a → p : 8.0, 9.0, 10.0, 11.0, 12.0, 13.0, 14.0, 15.0, 16.0, 17.0, 18.0, 19.0, 20.0, 21.0, 22.0, 23.0 mM; inset is the linear relationship of I$_{pc}$ versus H$_2$O$_2$ concentration).

NaNO$_2$ is an important detection object due to its particularly common in daily life and harmful to human body, which is imperative to establish a fast, efficient and sensitive means for NaNO$_2$ detection. Figure 5B showed the electrocatalytic reduction of NaNO$_2$ by Nafion/Mb/TiO$_2$@3DGR/CILE. A new reduction peak appeared at -0.755 V when NaNO$_2$ was gradually added to the pH 4.0 buffer and the corresponding I$_{pc}$ increased with C_{NaNO_2} from 0.5 to 9.0 mM. The linear regression equation was I (µA) = 13.07 C (mM) + 2.50 (n=11, γ=0.996) with the detection limit as 0.033 mM (3σ) and the K_M^{app} was 31.53 mM. The detection limit was smaller than the reported value of 0.15 mM [42] and 0.133 mM [43].

Figure 5C showed the electrocatalytic reductions of H$_2$O$_2$ by Nafion/Mb/TiO$_2$@3DGR/CILE. It was found that I$_{pa}$ and E$_{pa}$ gradually disappeared with I$_{pc}$ increased as H$_2$O$_2$ concentration range from 8.0 to 23.0 mM and E$_{pc}$ shifted negatively with the increased H$_2$O$_2$ concentration. The linear regression equation was I (µA) = 12.26C (mM) -67.34 (n=16, γ=0.998) with K_M^{app} of 34.23 mM and the detection limit of 0.033 mM (3σ), which was smaller than the report values of 0.1 mM [44] and 1.0 mM [45].

4. CONCLUSION

In this study, an electrochemical biosensor with TiO$_2$@3DGR and Mb as modifiers was constructed. The interaction between TiO$_2$@3DGR and Mb improved the signal response and enhanced the direct electrochemical behavior of the Mb molecule. The presence of TiO$_2$@3DGR accelerated the electrons transfer between the iron porphyrin inside the Mb molecule and the electrode surface. Electrocatalysis of TCA, NaNO$_2$ and H$_2$O$_2$ also had been studied with low detection limit and wide linear range. Thus, Nafion/Mb/TiO$_2$@3DGR/CILE can be used for the development of the third generation electrochemical biosensor.

References

1. P. Li, S. Y. Li, M. Liu, J. W. Ruan, Z. D. Wang, W. C. Xie, *Life Sci.,* 232 (2019) 116547.
2. D. Y. Xiao, H. Yi, W. Sheng, T. W. Gordon, G. I. Michael, Y. X. Zheng, *Acta Pharmacol. Sin.,* 39 (2018) 1155.
3. Y. T. Wang, L. Bao, B. Chu, S. Gao, M. Q. Lu, L. Shi, L. N. Fu, L. J. Fang, Q. Q. Xiang, *Cl. Lymph. Myelom. Leuk.,* 19 (2019) 167.
4. Q. L. Sheng, X. J. Qiao, M. Zhou, J.B. Zheng, *Microchim. Acta,* 184 (2017) 1573.
5. S. Palanisamy, C. Karuppiah, S. M. Chen, R. Emmanuel, P. Muthukrishnan, P. Prakash, *Sens. Actuators, B,* 202 (2014) 177.
6. W. B. Wei, S. Y. Dong, G. Y. Huang, Q. Xie, T. L. Huang, *Sens. Actuators, B,* 260 (2018) 189.
7. K. Xiao, L. X. Meng, C. C. Du, Q. Q. Zhang, Q. Yu, X. H. Zhang, J. H. Chen, *Sens. Actuator, B,* 328 (2021) 129096.
8. S. Kasturi, Y. J. Eom, S. R. Torati, C. G. Kim, *J. Ind. Eng. Chem.,* 93 (2021) 186.
9. F. J. Ren, T. Wang, H. T. Liu, D. S. Liu, R. Zhong, C. Y. You, W. J. Zhang, S. Y. Lv, S.S. Liu, H. Zhu, L. Chang, B. Wang, *Sep. Purif. Technol.,* 259 (2021) 118179.
10. F. Zhang, Y. Hua. L, J. Y. Li, Z. R. Tang, Y. J. Xu, *Environ. Pollut.,* 253 (2019) 365.
11. Z. Zhang, X. Du, Q. Wang, F. F. Gao, T. T. Jin, X. G. Hao, P. F. Ma, J. Li, G. Q. Guan, *Sep. Purif. Technol.,* 259 (2021) 118111.
12. J. Bai, J. Chu, X. J. Yin, J. R. Wang, W. Tian, Q. G. Huang, Z. M. Jia, X. L. Wu, H. X. Guo, Z. Qin, *Chem. Eng. J.,* 391 (2020) 123553.
13. W. H. Zhu, K. Kierzek, S. Wang, S. X. Li, R. Holze, X. C. Chen, *Colloids Surf. A,* 612 (2021) 126014.
14. R. W. Mo, D. Rooney, K. N. Sun, *Energy. Storage. Mater.,* 29 (2020) 198.
15. Q. K. Tan, S. C. Bao, X. L. Kong, X. Zheng, Z. G. Xu, Y. X. Hu, X. H. Liu, C. Wang, B. H. Xu, *J. Colloid Interface Sci.,* 590 (2021) 580.
16. B. Wang, Q. W. Liu, Z. Z. Fan, *Front. Chem.,* 8 (2020) 595643.
17. N. Song, X. Xie, D. Chen, G. F. Li, H. Z. Dong, L.Y. Yu, L. F. Dong, *J. Membr. Sci.,* 621 (2021) 118985.
18. M. Hao, W. Zeng, Y. Q. Li, Z. C. Wang, *Rare Met.,* 40 (2021) 1494.

19. J. H. Shin, M. J. Lee, J.H. Choi, J. A. Song, T. H. Kim, B.K. Oh, *Nano. Converg.,* 7 (2020) 39.
20. F. L. Liu, Z. Y. Kun, J. Q. Ding, T. T. Wen, X. W. Pei, Y. L. Yan, W. Ji, J. Liu, X. H. Zhang, L. Li, *Microchim. Acta,* 187 (2020) 574.
21. E. P. Lai, X. X. Yue, W. Ning, J. W. Huang, X. L. Ling, H. T. Lin, *Front. Chem.,* 7 (2019) 660.
22. X. Zhang , Y. X. Xu, M. C. Wang, E. Z. Liu, N. Q. Zhao, C. S. Shi, D. Lin, F. L. Zhu, C.N. He, *Nat. Commun.,* 11 (2020) 2775.
23. K. Xiang, T. Chen, Y. N. Wang, *Mater. Lett.,* 286 (2021) 129267.
24. K. H. Luo, C. K. Cheng, J. Y. Lin, C. H. Huang, T. K. Yeh, C. K. Hsieh, *Surf. Coat. Technol.,* 393 (2020) 125850.
25. L. Shen, J. Ying, L. Ren, Y. Yao, Y. Lu, Y. Dong, G. Tian, X. Y. Yang, B. L. Su, *J. Phys. Chem. Solids.,* 130 (2019) 1.
26. C. Fu, D. L. Yi, C. Deng, X. D. Wang, W. J. Zhang, Y. Tang, F. Caruso, Y. J. Wang, *Chem. Mater.,* 29 (2017) 5286.
27. D. Zhao, X. F. Zhang, W. J. Wang, L. L. Sui, C. Y. Guo, Y. M. Xu, X. L. Cheng, Z. Major, S. Gao, L.H. Huo, *Microchim. Acta,* 188 (2021) 74.
28. L. Y. Ge, R. Hou, Y. Cao, J. C. Tu, Q. Wu, *RSC Adv.,* 10 (2020) 44225.
29. M. T. Amiri, A. A. Ashkarran, *J. Mater. Sci.: Mater. Electron.,* 28 (2017) 9435.
30. X. R. Lü, P. Q. Hao, G. S. Xie, J. Y. Duan, L. Gao, B. X. Liu, *Sensors,* 19 (2019) 915.
31. H. Y. Xu, D. X. Ju, Z. R. Chen, R. Han, T. Zhai, H. Q. Yu, C. Y. Liu, X. W. Wu, J. Q. Wang, B. Q. Cao, *Sens. Actuator, B,* 273 (2018) 328.
32. M. I. Azmer, F. Aziz, Z. Ahmad, E. Raza, M. A. Najeeb, N. Fatima, T. M. Bawazeer, M. S. Alsoufi, R. A. Shakoor, K. Sulaiman, *Talanta,* 174 (2017) 279.
33. M. L. Zhang, T. Ning, P. Sun, D. Y. Zhang, Y. X. Yan, Z. M. Li, *Sens. Actuator, B,* 267 (2018) 565.
34. Y. Y. Niu, H. Xie, G. L. Luo, W. J. Weng, C. X. Ruan, G. J. Li, W. Sun, *RSC. Adv.,* 9 (2019) 4480.
35. X. L. Niu, H. Xie, G. L. Luo, Y. L. Men, W. l. Zhang, W. Sun, *J. Electrochem. Soc.,* 165 (2018) B713.
36. W. Sun, L. Li, B. Lei, T. Li, X. Ju, X. Wang, G. Li, Z. Sun, *Mater. Sci. Eng. C,* 33 (2013) 1907.
37. M. Jahanbakhshi, *Microchim. Acta,* 185 (2018) 121.
38. X. Q. Chen, H. Q. Yan, Z. F. Shi, Y. H. Feng, J. C. Li, Q. Lin, X. H. Wang, W. Sun, *Polym. Bull.,* 74 (2016) 75.
39. Y. X. Gu, Z. L.Tang, Y. Deng, L. Wang, *Electrochim. Acta,* 94 (2013) 165.
40. C. X. Yin, W. J. Weng, R. Gao, J. Liu, Y. Y. Niu, G. J. Li, W. Sun, *J. Chin. Chem. Soc.,* 66 (2019) 1341.
41. L. D. Kong, Z. Y. Du, Z. Y. Xie, R. J. Chen, S. H. Jia, R. X. Dong, Z. L. Sun, W. Sun, *Int. J. Electrochem. Sci.,* (2017) 2297.
42. C. Yu, H. Sun, S. F. Hou, *Anal. Methods*, 9 (2017) 4873.
43. Y. Y. Niu, X. Y. Li, H. Xie, G. L. Luo, R.Y. Zou, Y. R. Xi, G. J. Li, W. Sun, *J. Chin. Chem. Soc.,* 67 (2019) 1054.
44. H. Xie, X. Y. Li, G. L. Luo, Y. Y. Niu, R. Y. Zou, C. X. Yin, S. M. Huang, W. Sun, G. J. Li, *Diamond Relat. Mater.,* 97 (2019) 107453.
45. Y. Y. Niu, H. Xie, G. L. Luo, W. J. Weng, C. X. Ruan, G. J. Li, W. Sun, *RSC Adv.,* 9 (2019) 4480